

Understanding Electrolyte Ion Size Effects on the Performance of Conducting MOF Supercapacitors

Jamie W. Gittins^{1,‡}, Kangkang Ge^{2,‡}, Chloe J. Balhatchet¹, Pierre-Louis Taberna^{2,3}, Patrice Simon^{2,3*}, Alexander C. Forse^{1*}

¹ Yusuf Hamied Department of Chemistry, University of Cambridge, Lensfield Road, Cambridge CB2 1EW, UK.

² CIRIMAT, UMR CNRS 5085, Université Paul Sabatier Toulouse III, Toulouse 31062, France.

³ RS2E, Réseau Français sur le Stockage Electrochimique de l'Énergie, FR CNRS, 3459, Amiens Cedex 80039, France.

[‡] These authors contributed equally.

*Corresponding authors' emails: patrice.simon@univ-tlse3.fr, acf50@cam.ac.uk

Abstract

Layered metal-organic frameworks (MOFs) have emerged as promising materials for next-generation supercapacitors. Understanding how and why electrolyte ion size impacts electrochemical performance is crucial for developing improved MOF-based devices. To address this, we investigate the energy storage performance of $\text{Cu}_3(\text{HHTP})_2$ (HHTP = 2,3,6,7,10,11-hexahydroxytriphenylene) with a series of 1 M tetraalkylammonium tetrafluoroborate (TAABF_4) electrolytes with different cation sizes. Three-electrode experiments show that $\text{Cu}_3(\text{HHTP})_2$ exhibits higher energy storage upon positive charging and an asymmetric charging response with all ion sizes, with a greater charging asymmetry with larger TAA^+ cations. The results further show that smaller TAA^+ cations demonstrate superior capacitive performance upon both positive and negative charging compared to larger TAA^+ cations. To gain further insights, electrochemical quartz crystal microbalance (EQCM) measurements were performed to probe the ion electrosorption during charging. These reveal that $\text{Cu}_3(\text{HHTP})_2$ has a cation-dominated charging mechanism, but interestingly indicate that the solvent also participates in the charging mechanism with larger cations. Overall, the results of this study suggest that larger TAA^+ cations saturate the pores of the $\text{Cu}_3(\text{HHTP})_2$ -based electrodes, leading to more asymmetric charging and forcing solvent molecules to play a role in the charge storage mechanism. These findings significantly enhance our understanding of ion electrosorption in layered MOFs, and will guide the design of improved MOF-based supercapacitors.

Introduction

In recent years, electrically conductive layered MOFs have been synthesised with conjugated aromatic linker molecules.^{1,2} These materials, comprised of 2D π -d conjugated layers which stack to give a honeycomb structure, combine electrical conductivity with permanent porosity, making them promising electrode materials for energy storage applications.³⁻⁸ In particular, several layered MOFs have displayed encouraging capacitive performances in supercapacitors, underlining the potential of these frameworks in fast-charging energy storage devices.⁹⁻¹⁴ While recent work has attempted to improve the performances of MOF-based supercapacitors through optimisation of particle morphology,¹⁵⁻¹⁷ more studies are needed to further maximise device performances and to better understand the electrochemical behaviour of these emerging materials.¹⁸ Fortunately, the well-defined and tuneable structures of MOFs open the door to structure-performance studies that are difficult to perform with traditional porous carbon electrodes, facilitating the optimisation of MOF-based supercapacitors.

One design criterion that has not yet been optimised for layered MOF supercapacitors is the electrolyte ion size to electrode pore size ratio. Previous studies have attempted to answer this question for nanoporous carbon electrodes, although differences and difficulties in analysing the pore structure of carbon materials, which have amorphous and disordered structures, have led to conflicting and confusing results.¹⁹⁻²⁶ One effect observed in some studies on this topic is ‘porosity saturation’ of the porous carbon electrode.²⁷ This involves the complete filling of the electrolyte accessible surface area of the electrode during charging, and occurs when using electrolytes with larger ion sizes and carbons with low relative porosities. This tends to result in asymmetric charging, with a decreasing capacitance at high cell voltages due to saturation of the pores. These findings indicate that smaller ion sizes are favourable for higher performance when using electrode materials with lower total porosities than traditional porous carbons. While the impact of electrolyte ion size on the performances of porous carbons has been studied in detail, layered MOF electrodes remain underexplored,²⁸ with no studies looking at the impact of ion size on the performances of triphenylene-based MOFs which have been widely studied in the literature and display primarily double-layer capacitive behaviour. Such a study would provide insights into the ideal ion size for this family of materials, allowing for further optimisation of MOF-based systems. The well-defined structures of MOFs would also help to test general design principles for supercapacitors more widely.

Design principles for improved supercapacitors should be underpinned by a fundamental understanding of charging mechanisms. Such understanding provides deeper insights into why certain electrode and electrolyte combinations perform better than others, and could inspire new routes to increased performance. To date, only a few computationally-focussed studies have examined the charging mechanisms of MOF-based supercapacitors, with the first such study modelling the double-layer structure and charging process of Ni-based layered MOFs with a variety of pore sizes using molecular dynamics (MD) simulations.²⁹ More recently, Walsh *et al.* expanded on this by studying the electrochemical interface of the layered MOF $\text{Cu}_3(\text{HHTP})_2$ (HHTP = 2,3,6,7,10,11-hexahydroxytriphenylene) with tetraethylammonium tetrafluoroborate (TEABF_4) in acetonitrile

electrolyte using a multiscale quantum-mechanics/molecular-mechanics (QM/MM) approach.³⁰ In contrast to the previous approach, this accounted for the heterogeneous electronic structure of the MOF electrode and revealed how it changes with charging. Excitingly, comparison of simulated capacitance values, obtained for a range of different charging mechanisms, with experimental results indicated that cations are the dominant species participating in charge storage for $\text{Cu}_3(\text{HHTP})_2$, with minimal involvement of the anions. However, there has been a lack of experimental work to study the ion electrosorption in layered MOFs to confirm these findings.³¹ One technique that can be used to study ion adsorption during charging is electrochemical quartz crystal microbalance (EQCM), a technique that has been used extensively in nanoporous carbon and MXene devices to understand their charging mechanisms with a range of electrolytes.^{32–36} However, no studies have used EQCM to look at the double-layer charging of layered MOFs.^{8,28,31,37} Employing this technique to study the charge storage mechanisms of MOF-based devices alongside measurements of their electrochemical performance would allow the link between charging mechanisms and performance to be better understood.

Here, we present a detailed study examining the impact of electrolyte cation size on the capacitive performance and charge storage mechanism of the layered MOF $\text{Cu}_3(\text{HHTP})_2$, which has a well-defined unimodal pore size distribution. We find that smaller cations result in higher capacitive performances upon both positive and negative charging, with highly asymmetric charging seen with larger cations. EQCM measurements suggest a cation-dominated charging mechanism for this series of tetraalkylammonium (TAA^+) electrolytes, with potential involvement of the solvent for electrolytes with larger cation sizes. Overall, our findings indicate that larger electrolyte cations lead to porosity saturation in the MOF electrodes, resulting in more asymmetric charging and lower overall energy storage performance. This is the first work to examine the charging mechanisms of a layered MOF supercapacitor using operando EQCM, and it demonstrates that smaller electrolyte ions lead to higher capacitive performances in MOF-based supercapacitors.

Results & Discussion

Materials Synthesis & Characterisation

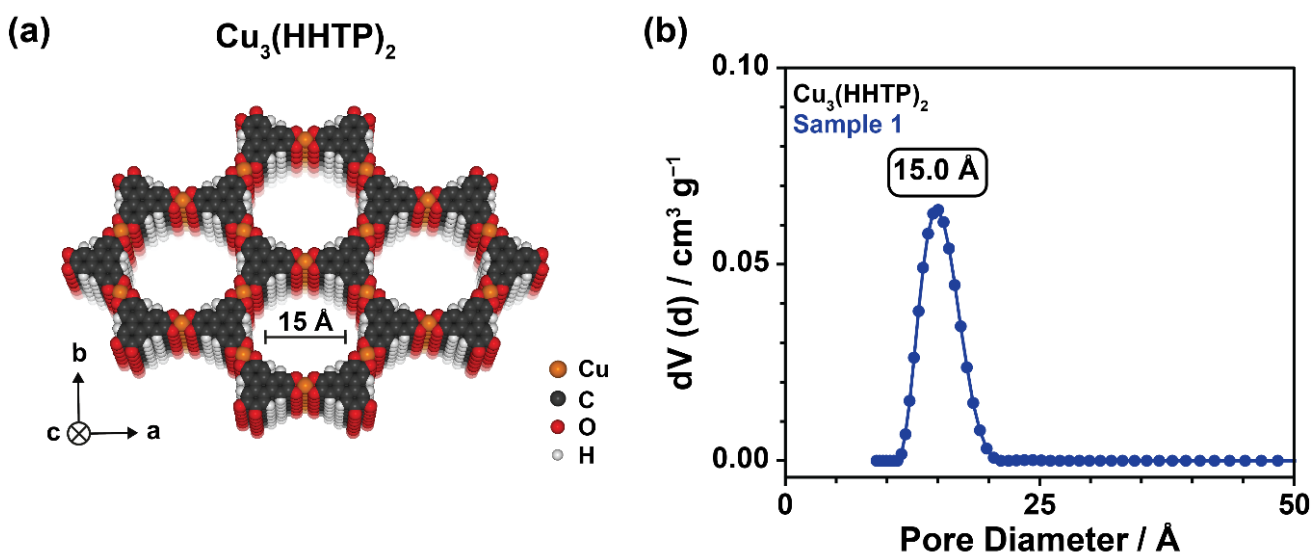


Figure 1: (a) Schematic showing the structure of the conductive layered MOF $\text{Cu}_3(\text{HHTP})_2$, along with (b) the pore size distribution of $\text{Cu}_3(\text{HHTP})_2$ calculated from a N_2 sorption isotherm using a N_2 at 77 K on carbon (cylindrical pores) quenched solid density functional theory (QSDFT) model. This shows the unimodal and well-defined pore structure of this framework, centred at approximately 15 Å. The 77 K N_2 sorption isotherm for this sample is shown in SI Figure S3.

The layered MOF $\text{Cu}_3(\text{HHTP})_2$ (**Fig. 1a**) was chosen as the model electrode material for this study as it has a well-defined pore size and structure, and its electrochemical performance has been characterised in detail in previous work.^{14,15} Polycrystalline samples of $\text{Cu}_3(\text{HHTP})_2$ were synthesised using a previously reported literature synthesis (see Supplementary Information),¹¹ and the chemical composition of the framework was confirmed by elemental analysis, which revealed the expected ratio of Cu and HHTP (SI Table 1). Elemental analysis also showed that some nitrogen-containing impurities remain in the framework after extensive washing and activation, consistent with previous reports.^{14,38} Scanning electron microscopy (SEM) confirmed that the use of ammonia as a modulator in the synthesis resulted in the formation of flake-like crystallites, which were previously shown to be the crystal morphology that exhibits the best performance in $\text{Cu}_3(\text{HHTP})_2$ supercapacitor devices (SI Fig. S1).¹⁵

PXRD patterns confirmed the high crystallinity of as-synthesised $\text{Cu}_3(\text{HHTP})_2$ (SI Fig. S2) and indicated that this material has a hexagonal eclipsed unit cell with AA layer stacking. Unit cell parameters of $a \approx b = 21.2 \text{ \AA}$, and an interlayer spacing $c = 3.1 \text{ \AA}$ were calculated from the PXRD patterns. This leads to a predicted crystallographic pore size of 16 Å. The pore size distribution of this material, along with its porosity, were further analysed using 77 K N_2 sorption isotherms (SI Fig. S3). Brunauer-Emmett-Teller (BET) analysis on two independent samples confirmed that the material synthesised in this work is highly porous, with a BET surface area of $802 \pm 40 \text{ m}^2 \text{ g}^{-1}$ obtained.³⁹ Importantly, pore size distribution (PSD) analysis confirmed that $\text{Cu}_3(\text{HHTP})_2$ has an ordered, unimodal pore size distribution centred at 15.0 Å (**Fig. 1b**), in good agreement with the

crystallographic pore size. This further confirms the well-defined long-range order of this material. This is in contrast to porous carbons, which have significantly more disordered structures with little long-range ordering and broad pore size distributions (SI Fig. S4). Overall, this supports the use of layered MOFs, such as $\text{Cu}_3(\text{HHTP})_2$, to establish structure-performance relationships in supercapacitors.

PXRD and N_2 sorption analysis confirmed that the long-range order and porosity of $\text{Cu}_3(\text{HHTP})_2$ is largely maintained upon forming a composite electrode film with PTFE and a conductive additive for use in electrochemistry experiments (SI Fig. S5, S6). However, the N_2 sorption analysis reveals a decrease in the porosity of $\text{Cu}_3(\text{HHTP})_2$ in the electrode films, with a BET area of $545 \pm 7 \text{ m}^2 \text{ g}^{-1}$ calculated for the constituent $\text{Cu}_3(\text{HHTP})_2$ after removing the contribution of acetylene black and assuming PTFE does not contribute to the adsorption. This represents a decrease in the surface area of $\text{Cu}_3(\text{HHTP})_2$ of approximately 32% compared to powder samples. Furthermore, there is a slight reduction in the modal pore size to $14 - 14.2 \text{ \AA}$. This shows that PTFE and/or acetylene black are blocking some of the pores and reducing the available surface area of the MOF. While infiltration of polymers into the pores of MOFs has been observed previously using NMR,⁴⁰ this effect had not previously been quantified for conductive layered MOFs. While a decrease in porosity has also been observed for porous carbon materials when made into composite electrode films, the percentage decrease in surface area was much smaller.^{41,42} This was confirmed in this work, where a decrease of 4% in the BET area of YP80F was observed upon formation of an electrode film (SI Fig. S7). This suggests that the binder and conductive additive are significantly more effective at blocking the ordered one-dimensional porosity in layered MOFs. Optimisation of layered MOF composite electrode films, by changing both the conductive additive and binder, may help to minimise this effect and improve the performances of these materials in supercapacitors. Having confirmed the well-defined structure of $\text{Cu}_3(\text{HHTP})_2$, we proceeded to use this layered MOF to probe the cation size-performance relationship.

Three-Electrode Energy Storage Measurements of $\text{Cu}_3(\text{HHTP})_2$

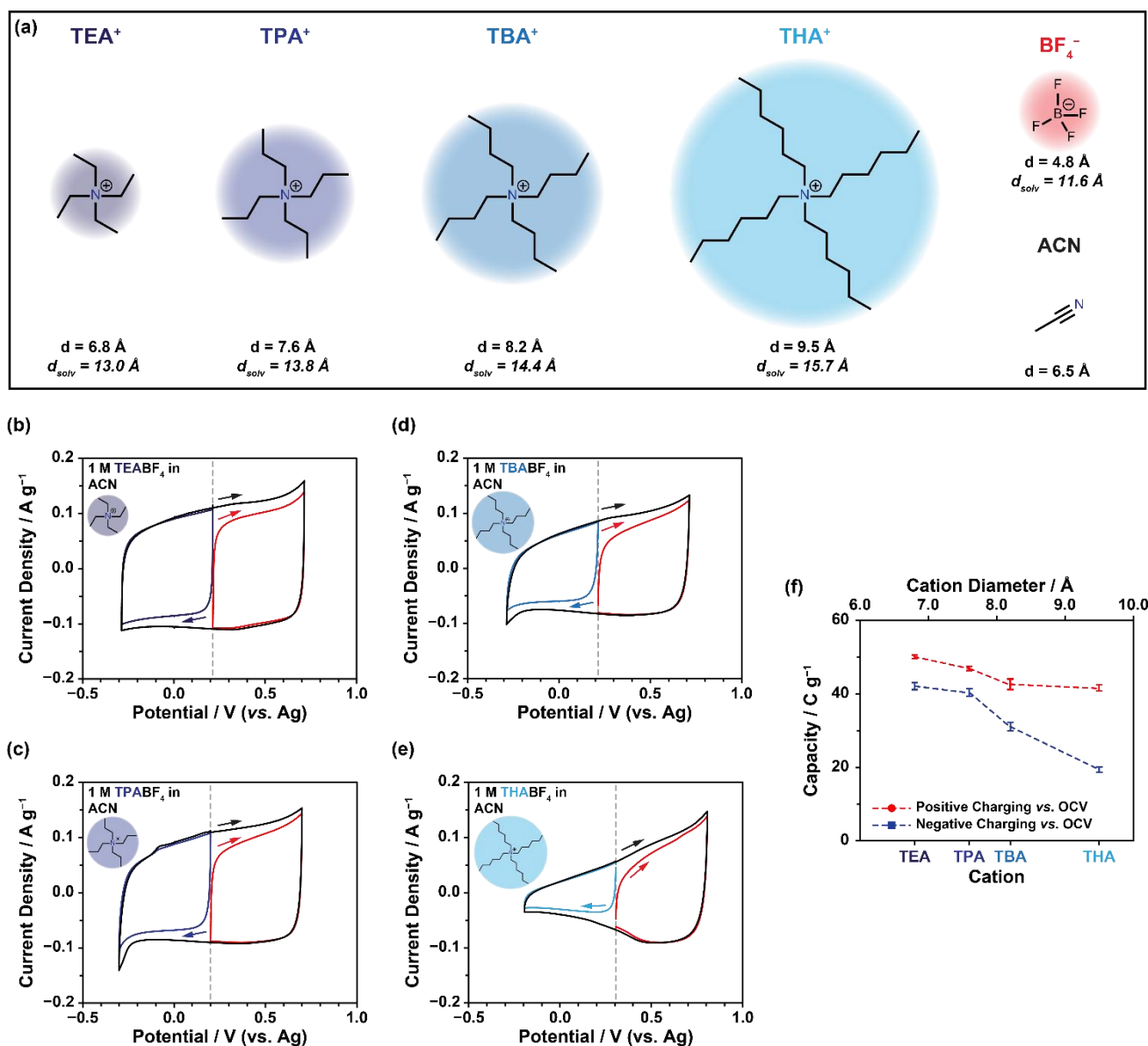


Figure 2: (a) The Lewis structure of each tetraalkylammonium (TAA⁺) cation, along with the naked and solvated ion sizes, for each electrolyte species used in this study. The solvated ion sizes are calculated assuming a primary solvation shell of acetonitrile molecules.^{47,57–59} (b) – (e) Cyclic voltammetry (CV) data obtained at a scan rate of 1 mV s⁻¹ from three-electrode cells assembled with $\text{Cu}_3(\text{HHTP})_2$ working electrodes, YP80F oversized counter electrodes, and Ag pseudo-reference electrodes, with 1 M solutions of (b) TEABF₄, (c) TPABF₄, (d) TBABF₄, and (e) THABF₄ in acetonitrile as electrolytes. The open circuit voltage (OCV) is indicated by the dashed line. Data was acquired by scanning to +0.5 V vs. OCV (positive charging; red), -0.5 V vs. OCV (negative charging; blue), and across the full potential window (black). $\text{Cu}_3(\text{HHTP})_2$ was stable and showed minimal Faradaic peaks between the chosen potential limits for each electrolyte, confirming mainly double-layer charge storage for each electrolyte in this potential range. The direction of scanning is indicated by the arrow in each case. (f) Specific capacity values calculated from galvanostatic charge-discharge (GCD) profiles at a current density of 0.05 A g⁻¹ when charging to +0.5 V vs. OCV (red) and -0.5 V vs. OCV (blue). The red and blue dashed lines are added as guidelines. The mass of $\text{Cu}_3(\text{HHTP})_2$ in the working electrode was used to calculate specific capacity values. This shows how the charge storage changes with cation size for both positive and negative charging.

The impact of ion size on the energy storage performance of $\text{Cu}_3(\text{HHTP})_2$ was studied by using a series of 1 M tetraalkylammonium tetrafluoroborate (TAABF_4) in acetonitrile electrolytes (**Fig. 2**). While all electrolytes had the same anion (BF_4^-), and thus a constant anion size (4.8 Å naked; 11.6 Å solvated)⁴³, the TAA^+ cation was varied to systematically change the cation size. In total, four different cations were used: tetraethylammonium (TEA^+), tetrapropylammonium (TPA^+), tetrabutylammonium (TBA^+) and tetrahexylammonium (THA^+), with their naked and solvated sizes summarised in **Figure 2a**. This allowed for a variation in unsolvated cation size between 6.8 – 9.5 Å (solvated: 13.0 – 15.7 Å).^{43,44} A three-electrode arrangement enabled the response of $\text{Cu}_3(\text{HHTP})_2$ upon both negative and positive charging relative to the open circuit voltage (OCV) to be studied separately (**Fig. 2b–e**; SI Fig. S8). To evaluate the charge storage, specific capacity and specific capacitance, C_g , were calculated (**Fig. 2f**; SI Table S2 and S3; and SI Fig. S9). All experimental capacity and capacitance values for $\text{Cu}_3(\text{HHTP})_2$ were calculated after removing the contributions of acetylene black and PTFE that are also present in the electrodes. Capacity is reported as the primary energy storage performance metric in this work rather than capacitance due to the non-linearity of the GCD discharge curves produced from these systems. This is in accordance with previous recommendations on data analysis.⁴⁵ Low current densities and scan rates were used to attempt to ensure complete permeation of the ions into the MOF pores and to minimise the impact of differences in ion kinetics on the results.

Both CV and GCD three-electrode experiments reveal exciting insights into the cation size-performance behaviour of $\text{Cu}_3(\text{HHTP})_2$. Firstly, an overall decrease in capacity for both positive and negative charging was observed as the solvated electrolyte cation size approaches and then exceeds the electrode pore size of approximately 14 Å (**Fig. 2f**), with TEA^+ having the highest capacity for both positive and negative charging. This result demonstrates that smaller electrolyte ions lead to higher energy storage performances in MOF-based supercapacitors, and represents the first time that the impact of ion size on the performances of triphenylene-based conductive layered MOFs has been uncovered. One potential explanation for this cation size-performance behaviour is that the nitrogen charge centre of the smaller TAA^+ cations can get closer to the pore walls of $\text{Cu}_3(\text{HHTP})_2$, resulting in smaller charge separation distances and higher capacities.^{19,20} These results confirm, as expected, that electrolytes with smaller ion sizes should be employed in conductive layered MOF supercapacitors in the future to optimise their energy storage performances.

The CV data also shows that $\text{Cu}_3(\text{HHTP})_2$ displays a clear asymmetric charging response with all TAA^+ electrolytes, with the capacity upon positive charging greater than the capacity upon negative charging (**Fig. 2b–e**). It is worth noting that there is an increase in the degree of asymmetry as the cation size increases, with a significant increase from TPA^+ to TBA^+ , and THA^+ having the greatest difference in capacity between positive ($41.6 \pm 1.4 \text{ C g}^{-1}$) and negative ($19.5 \pm 1.4 \text{ C g}^{-1}$) charging. Interestingly, this charging behaviour is reminiscent of porosity saturation that has been observed previously in low porosity carbon electrodes with electrolytes with large cations.²⁷ These systems also exhibit asymmetric charging, with a significant decrease in charge storage at high cell voltages as the carbon pores become saturated by large TAA^+ cations during charging. Porosity saturation in $\text{Cu}_3(\text{HHTP})_2$ is plausible due to the relatively low total porosities of the MOF electrode films compared to other traditional supercapacitor electrode materials, such as porous carbons.^{30,41,42} While there is

only a small decrease in the negative charging capacity when increasing the cation size from TEA⁺ ($42.1 \pm 1.9 \text{ C g}^{-1}$) to TPA⁺ ($40.4 \pm 2.0 \text{ C g}^{-1}$), there is a much larger drop in capacity between TPA⁺ and TBA⁺ ($31.2 \pm 2.0 \text{ C g}^{-1}$). This strongly suggest that porosity saturation only becomes significant for cation sizes of TBA⁺ and above, and provides another explanation for the higher charge storage performances of smaller cations noted above. Three-electrode rate capability and electrochemical impedance spectroscopy (EIS) measurements support this hypothesis, as both measurements indicate large decreases in ion mobility during negative charging for TBA⁺ and THA⁺ compared to TEA⁺ and TPA⁺, consistent with the larger cations struggling to fit into the near-saturated pore network of the electrodes (SI Fig. S9–S11; SI Table S3). Ion sieving, a related phenomenon which has been seen in other layered materials, also gives rise to similar asymmetric charging behaviour,^{46–48} but is unlikely in these systems as the naked (desolvated) cation sizes are all significantly smaller than the electrode pore size.

Electrochemical experiments on symmetric two-electrode supercapacitors assembled with this series of electrolytes support the above findings (SI Fig. S12–S14; SI Table S4). Once again, TEA⁺ showed the best energy storage performance with Cu₃(HHTP)₂, supporting the conclusion that smaller electrolyte ions are favourable for high capacitive performances with this class of materials. In addition, a large drop in performance was seen between TPA⁺ and TBA⁺, providing further evidence for porosity saturation with larger TAA⁺ cations. The asymmetric charging behaviour of these systems has additional consequences for symmetric two-electrode cells. For electrolytes with larger cations, differences in capacity between the two oppositely polarised electrodes results in the potential of the negative electrode going outside its stable potential window. This leads to quasi-reversible Faradaic activity at lower cell voltages, resulting in more facile degradation of Cu₃(HHTP)₂ and reducing the energy density of devices with larger cations (SI Fig. S12). This further highlights the superior performance of smaller TAA⁺ cations with Cu₃(HHTP)₂. To investigate these results in more detail and better understand the impact of cation ion size on the performance of Cu₃(HHTP)₂, EQCM was used to probe the ion flux and charging mechanisms of these systems.

EQCM Studies of the Charging Mechanism

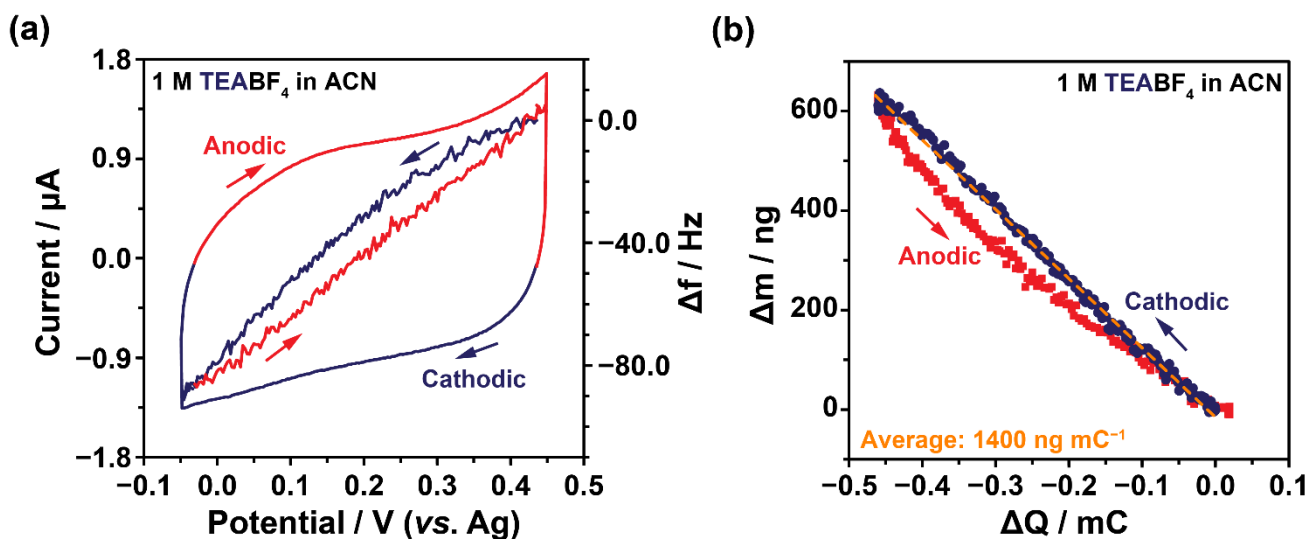


Figure 3: (a) CV and EQCM frequency response of $\text{Cu}_3(\text{HHTP})_2$ with 1 M TEABF_4 in a acetonitrile electrolyte, obtained at a scan rate of 1 mV s^{-1} in the potential range from -0.05 to $+0.45 \text{ V vs. Ag}$. This potential range was chosen to avoid non-capacitive processes that occur on the quartz surface at low scan rates. All EQCM cells were assembled with $\text{Cu}_3(\text{HHTP})_2$ -coated quartz working electrodes, platinum wire counter electrodes, and Ag pseudo-reference electrodes. (b) Plot of electrode mass change, calculated from the frequency response shown in (a), against accumulated charge (ΔQ). ΔQ was calculated by integrating the current against time for the CVs, and setting the charge at the electrode potential of $+0.45 \text{ V vs. Ag}$ to zero. The frequency response and mass change are considered separately for cathodic (blue) and anodic (red) polarisations. The dashed line (orange) shows the average mass change during the full CV experiment. The OCV of the cell used to produce the data in the figure above was $+0.16 \text{ V vs. Ag}$.

EQCM studies were initially performed on $\text{Cu}_3(\text{HHTP})_2$ with 1 M TEABF_4 in acetonitrile electrolyte (Fig. 3). The CV was sub-divided into two sections based on the polarisation of the electrode: a cathodic regime with a negative current response ($I < 0$), and an anodic regime with a positive current response ($I > 0$) (Fig. 3a; outside lines). EQCM cells with TEA^+ were cycled between the potential limits of $+0.29 \text{ V vs. OCV}$ to -0.21 V vs. OCV . Although the potential window is narrower than that used in the three-electrode experiments above, it covers both positive and negative charging as defined for Figure 2b, allowing the charging mechanism to be studied for both charging directions. The lower stable potential window of the EQCM cell was due to instabilities of the gold coating and its related titanium adhesion layer on the quartz crystal outside the chosen potential limits. Also shown in Figure 3a (inside lines) is the change in resonance frequency response, Δf , of the $\text{Cu}_3(\text{HHTP})_2$ -coated quartz crystal during the CV experiment. In this work, Sauerbrey's equation applies as there was negligible change in motional resistance (ΔR) during CV cycling for the EQCM cells (SI Fig. S15, S17). As a result, Δf of the $\text{Cu}_3(\text{HHTP})_2$ -coated quartz crystal was translated into a mass change (Δm) of the working electrode during the cycling, where an increase in Δm corresponds to a decrease in Δf (see SI for details).⁴⁹ Δm was then plotted against the accumulated electronic charge, ΔQ (Fig. 3b) to allow analysis of the charging mechanism in greater detail, including assigning the different species entering and leaving the electrode pores during charging and discharging. If Δm is negatively correlated with ΔQ , cations ("counterions") are the main charge carriers, while the opposite stands for a positive correlation.

TEABF₄ showed an approximately rectangular EQCM CV response, consistent with the above three-electrode experiments (**Fig. 3a**). The $\Delta m-\Delta Q$ plot for this system demonstrates a reversible and linear mass change during cycling, with the mass change upon both cathodic (negative) and anodic (positive) charging aligning closely to the average value (dashed orange line, **Fig. 3b**). This suggests a kinetically reversible process with the same dominant charge carrier for both charging directions. As the slope of the $\Delta m-\Delta Q$ plot is negative, this indicates that cation (counterion) adsorption and desorption are the dominant charge storage mechanisms. If anions (co-ions) were involved in the charging mechanism, as would be the case for an ion exchange mechanism, there would be an obvious decrease in the slope of the $\Delta m-\Delta Q$ with charge accumulation, resulting in a weaker $\Delta m-\Delta Q$ correlation. Both the cathodic and anodic charging regimes show an average mass change close to 1400 ng mC⁻¹, corresponding to an equivalent molecular weight of 139 ± 4 g mol⁻¹ (SI Fig. 16). This aligns closely with the molecular weight of the naked TEA⁺ ion (130 g mol⁻¹), and further confirms that the cations are the dominant charge carriers across the full potential range considered here. As the experimental mass change is consistent with adsorption and desorption of naked TEA⁺ cations, this charging mechanism would require no net movement of anions or solvent molecules in or out of the electrode pores. However, the solvated ion size of TEA⁺ (13.0 Å) in the bulk electrolyte²⁷ is less than the average pore size of Cu₃(HHTP)₂ in the electrode film (~14 Å), indicating that solvated TEA⁺ cations are still able to enter and leave the pores of the MOF. If this were to occur during the charging mechanism, an equivalent amount of free solvent molecules would need to leave or enter the pores. This demonstrates a key limitation of EQCM experiments as the contributions of different electrolyte species to the net mass change cannot be distinguished. Overall however, our EQCM results suggest that cation desorption (positive charging) and cation adsorption (negative charging) are the primary charging mechanisms for Cu₃(HHTP)₂ in 1 M TEABF₄ in the potential range from -0.05 V to +0.45 V vs. Ag (**Fig. 4**). This is in contrast to the double-layer charge storage mechanism of traditional porous carbons, where both the anions and cations have been shown to play a role in the charging mechanisms.^{32,34,50} This finding also begins to explain our capacity data in **Figure 2b-e**, where variation in the size of the cation (*i.e.* the dominant charge carrier) impacted the capacitance for *both* positive and negative charging in the present potential window. Excitingly, this finding is in line with recent computational work on this system, which suggested a cation-dominated charging mechanism for this system.³⁰

Although the EQCM results suggest that the anions are not involved in the charging mechanism, their involvement cannot be ruled out. Simulations from Walsh *et al.* found that, while TEA⁺ cations only have one possible adsorption site in the pores of Cu₃(HHTP)₂, BF₄⁻ anions have two environments: a weaker binding site at the centre of the pore, and a stronger binding site at the pore edge where the BF₄⁻ anions interact with the C-H moieties of the HHTP linker molecules (**Fig. 4**).³⁰ At the OCV, the simulations showed that anions exist in both environments. However, upon positive charging (cation desorption), simulations found that the anions shift and predominantly occupy the more strongly bound edge site. Upon negative charging (cation adsorption), the opposite occurs with the anions shifting to occupy the pore centre site. However, as there is no net change in the in-pore population of BF₄⁻ from this process, and thus no net anion flux, EQCM is not able to detect this potential contribution of the anions to the charging mechanism, although it is likely to be a more minor contribution to the overall charge storage compared to the adsorption/desorption of cations. This illustrates that a multi-technique

approach is required to get a complete picture of charging. Other experimental techniques, such as NMR spectroscopy, should be used to better understand the role of both the anions and solvent in the charging mechanism of this system.^{51,52}

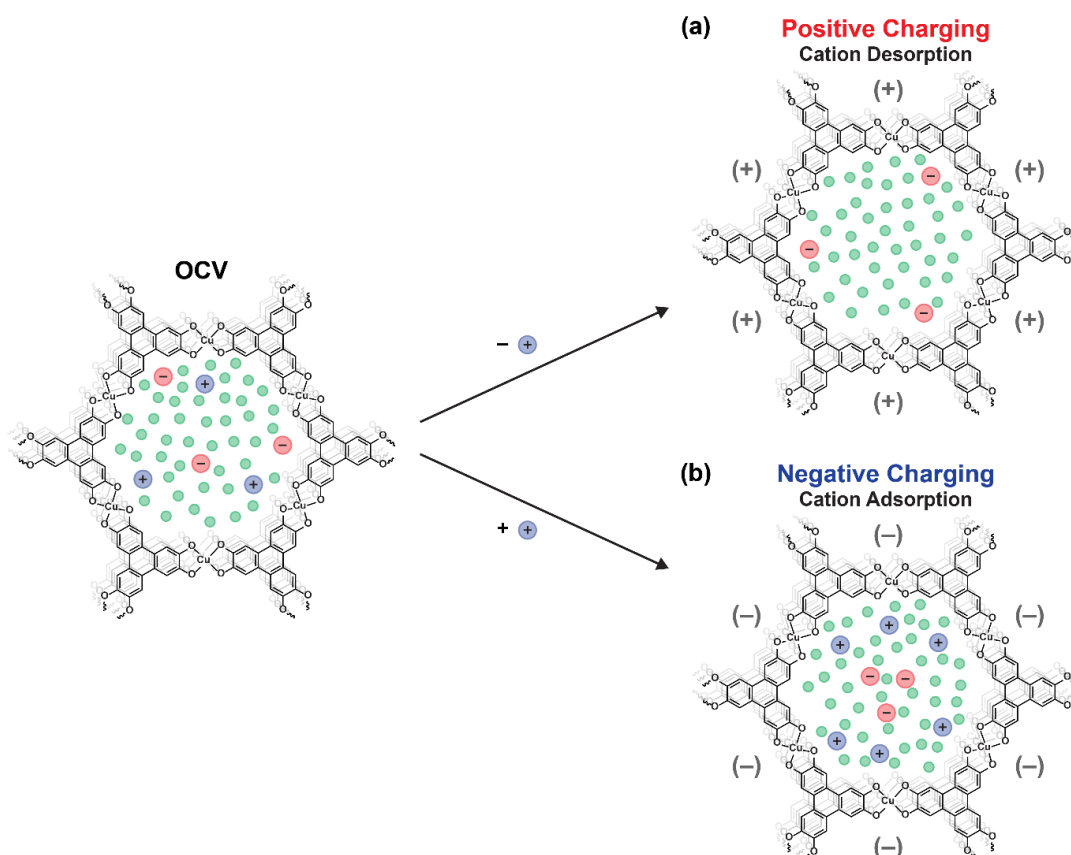


Figure 4: Cartoon of the cation-dominated charging mechanism of CuHHTP with 1 M TEBABF₄ in acetonitrile, as deduced from EQCM and computational studies.³⁰ (a) Upon positive charging, there is cation desorption from the MOF pores, with the anions shifting to a more strongly interacting edge adsorption site. (b) Upon negative charging, the reverse occurs with cation adsorption and corresponding movement of the anions to the more weakly bound centre adsorption site. Note that the ion and solvent sizes are not to scale, and the solvation of electrolyte ions is not shown.

Building on the results with TEABF₄, EQCM studies were also performed with 1 M THABF₄ in acetonitrile electrolyte to assess how the charging mechanism changes upon increasing the cation size, and to provide insights into why larger cations lead to lower energy storage performances with Cu₃(HHTP)₂ (**Fig. 5**). Negligible change in motional resistance (ΔR) was also observed with this electrolyte. EQCM cells with THA⁺ were cycled between the potential limits of +0.23 V *vs.* OCV to -0.27 V *vs.* OCV, allowing for investigation of the charge storage mechanism for both positive and negative charging as defined for **Figure 2e**. As observed in the 3-electrode measurements, THA⁺ exhibited an asymmetric CV (**Fig. 5a**), resulting in an asymmetric Δm - ΔQ plot that displays a clear mass hysteresis about the average mass change of 1250 ng mC⁻¹ (dashed orange line; **Fig. 5b**). This indicates clear differences in the charging mechanism between the cathodic and anodic charging regimes (**Fig. 5b**), in contrast with the results for TEA⁺ (**Fig. 3b**).

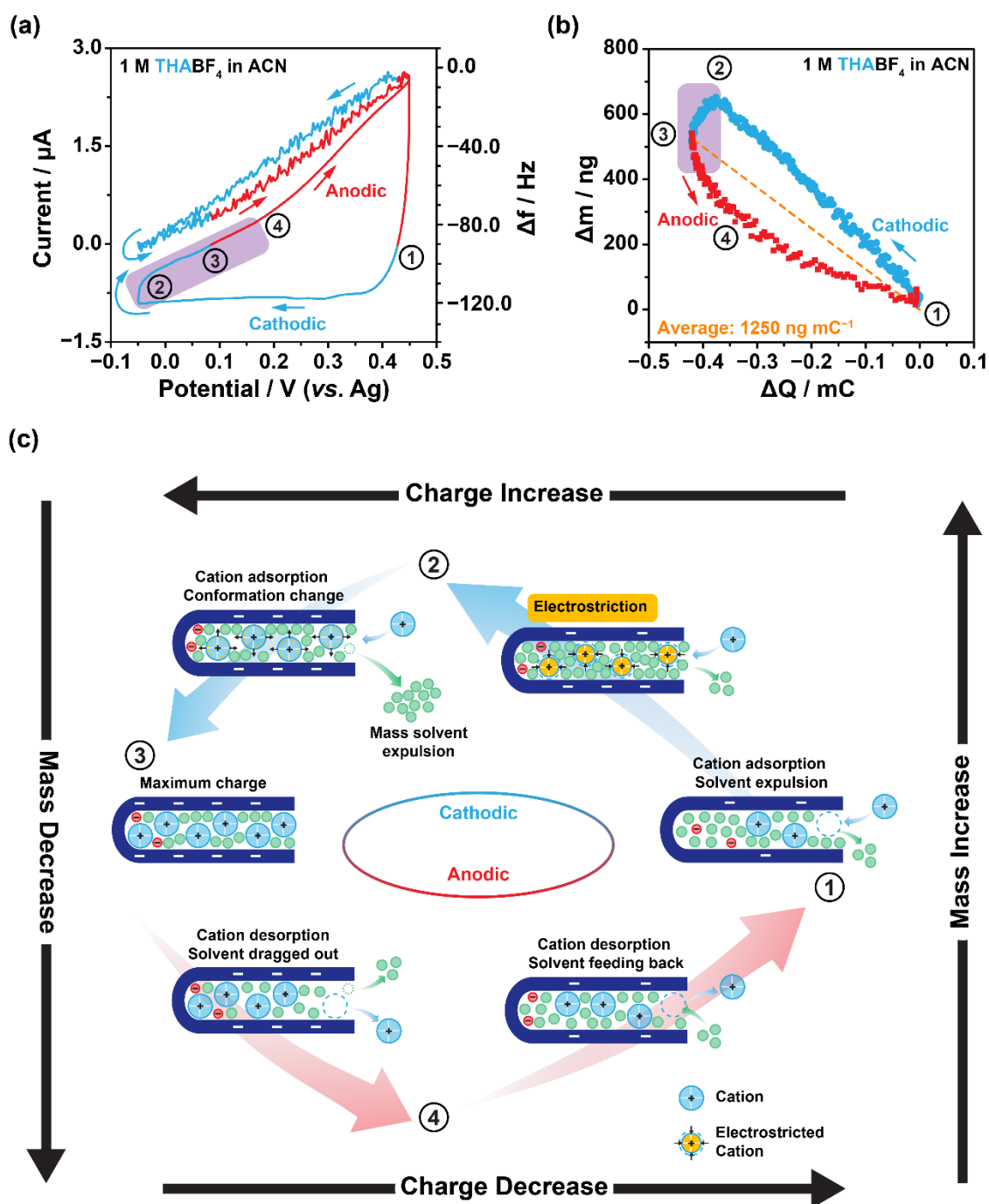


Figure 5: (a) CV and EQCM frequency response of $\text{Cu}_3(\text{HHTP})_2$ with 1 M THABF₄ in acetonitrile electrolyte, obtained at a scan rate of 1 mV s^{-1} in the potential range from -0.05 to $+0.45 \text{ V vs. Ag}$. All EQCM cells were assembled with $\text{Cu}_3(\text{HHTP})_2$ -coated quartz working electrodes, platinum wire counter electrodes, and Ag pseudo-reference electrodes. (b) Plot of electrode mass change, calculated from the frequency response shown in (a), against an accumulated charge. The frequency response and mass change are considered separately for positive (cathodic, shown in blue) and negative (anodic, shown in red) polarisations. The dashed line (orange) shows the average mass change during the full CV experiment, calculated from Faraday's law. The abnormal mass drop is highlighted in violet. The OCV of the cell used to produce the data in the figure above was $+0.22 \text{ V vs. Ag}$. (c) Cartoon schematic of the possible charging mechanism of $\text{Cu}_3(\text{HHTP})_2$ with 1 M THABF₄, showing cation and solvent movement upon cathodic charging and anodic discharging. Note that the solvation of electrolyte ions is not shown.

During the cathodic scan from $\Delta Q = 0$ to $\Delta Q = -0.38$ mC, there is an approximately linear increase in Δm with an average slope of 1660 ng mC⁻¹ (**Fig. 5b**). However, the equivalent molecular weight corresponding to this mass increase was calculated to be only 163 ± 3 g mol⁻¹ (SI Fig. S18), less than the molecular weight of the naked THA⁺ cation (298 g mol⁻¹). If this was due to involvement of anions in the charging process, a parabolic-like $\Delta m - \Delta Q$ plot would be expected, with an increasing slope as the total charge increases.⁵³ However, as the mass change is approximately linear, and there's a negative correlation with ΔQ , it is likely that the anions do not play a significant role in the charge storage mechanism. Instead, involvement of solvent in the charging process is a more likely explanation for the lower observed mass change, and is consistent with a linear $\Delta m - \Delta Q$ plot. Therefore, the results suggest that cation insertion is accompanied by a net loss of solvent molecules from the electrode pores during cathodic charging, with adsorption of one THA⁺ cation accompanied by the loss of 3.3 acetonitrile molecules on average (**Fig. 5c**; process from stage 1 to 2). This observation supports the hypothesis of porosity saturation in Cu₃(HHTP)₂ when charging with larger TAA⁺ cations, with a net expulsion of solvent molecules from the pores required following cation adsorption upon cathodic charging, resulting in lower observed equivalent molecular weight changes.

Porosity saturation is further supported by examining the mass change in the potential range from -0.05 V to $+0.22$ V vs. Ag. In this region, a steep mass drop is observed (purple box; **Fig. 5b**). This behaviour is not seen with TEA⁺, and is once more indicative of overcrowding of the electrode pores with THA⁺. One potential explanation for this unexpected mass drop is a conformational change of the large THA⁺ cations upon a change in polarisation at high accumulated charges. At the start of the cathodic scan (**Fig. 5c**; stage 1), THA⁺ cations with long flexible alkyl chains start to accumulate in the pores, resulting in a significant increase in the in-pore cation density. As a result, the tightly packed THA⁺ cations become electrostricted at high negative polarisations. However, when the polarisation is reversed at -0.05 V (**Fig. 5c**; stage 2 to 3), the release of electrostatic force drives a change in conformation of the electrostricted THA⁺ cations from a compact packing to a looser packing arrangement. Similar behaviour is observed in surface-active ionic liquids with analogous structures.⁵⁴⁻⁵⁶ This conformational change is accompanied by an increase in volume of the in-pore cations, resulting in an expulsion of solvent molecules from the saturated MOF pores and a sudden mass decrease. At the maximum accumulated charge (**Fig. 5c**; stage 3), the in-pore cation population reaches a maximum and the in-pore solvent number reaches minimum. This results in a highly concentrated in-pore ion population, leading to considerable steric hindrance between the long alkyl chains of THA⁺ and thus slower ion kinetics, evidenced by the resistive current response from stage 2 to 4 (purple box; **Fig. 5a**). Poorer kinetic performance with THA⁺ is also seen in both rate capability and electrochemical impedance spectroscopy (EIS) measurements on three-electrode cells (SI Fig. S9, S10), supporting lower ion mobility of the larger TAA⁺ cations.

At the start of anodic charging (**Fig. 5c**, stage 3 to 4), desorption of THA⁺ cations occurs and is accompanied by loss of solvent molecules. This leads to a pronounced observed mass loss in this region (**Fig. 5b**). However, as anodic charging continues and more desorption of large THA⁺ cations from the MOF pores occurs, the amount of free in-pore volume significantly increases. As a result, solvent molecules can feed back into the electrode pores from the bulk electrolyte as cation desorption

continues (**Fig. 5c**; stage 4 to 1). This leads to a gradual reduction in the slope of the $\Delta m-\Delta Q$ plot in this region (**Fig. 5b**). Due to this phenomenon, there is a corresponding improvement in ion kinetics between stages 4 and 1, evidenced by the increased anodic current in this region (**Fig. 5a**). However, as for TEA^+ , the possibility of anion involvement in the charging mechanism with THA^+ cannot be fully ruled out as EQCM gives only a net mass change and cannot distinguish between different species.

Summarising, the EQCM results illustrate that the charging mechanism significantly changes as the cation size is increased from TEA^+ to THA^+ . Furthermore, these results support the hypothesis from electrochemical measurements of porosity saturation in $\text{Cu}_3(\text{HHTP})_2$ when charging with larger TAA⁺ cations, with a significantly lower available pore volume following cation adsorption forcing the solvent to participate in the charge storage mechanism. This surprising change has not been observed in other supercapacitor systems. Together with the three-electrode measurements, this demonstrates that porosity saturation can occur in $\text{Cu}_3(\text{HHTP})_2$ electrodes with large electrolyte ions, resulting in both asymmetric charging and lower capacities. This is perhaps unsurprising given the comparatively lower total pore volume of layered MOF composite films compared to those of most traditional porous carbons. As a result, electrolytes with small ion sizes should be used to maximise the performance of MOF-based supercapacitors. Additionally, this work also demonstrates the crucial significance of operando EQCM in elucidating ion transport mechanisms under nanoconfinement.

Conclusion

In summary, this study has probed both the ion-size performance relationship and the charging mechanism of the layered MOF $\text{Cu}_3(\text{HHTP})_2$ to provide a detailed description of the electrochemical behaviour of this material. Three-electrode measurements revealed that smaller cations result in higher charge storage performances upon both positive and negative charging, showing that electrolytes with small ion sizes should be employed in layered MOF supercapacitors to maximise their performances. Furthermore, our results indicate that porosity saturation of the $\text{Cu}_3(\text{HHTP})_2$ electrode occurs when using electrolytes with larger TBA^+ and THA^+ cations. Charging mechanism studies with EQCM support these findings. These measurements revealed that $\text{Cu}_3(\text{HHTP})_2$ exhibits a cation-dominated charging mechanism with TEABF_4 , the electrolyte with the smallest cation used in this study, with co-ion desorption upon positive charging and counterion adsorption upon negative charging. No net movement of the solvent or anions in or out of the electrode pores was observed for this system. However, with THABF_4 , EQCM indicated that solvent molecules also likely participate in the charging mechanism, illustrating that increasing the cation size changes the charging mechanism of MOF-based supercapacitors. This result further supports saturation of the MOF pores with larger electrolyte ions, and confirms that electrolytes with smaller ion sizes should be targeted to optimise the performances of MOF-based devices going forwards. Our findings on this crystalline electrode system with unimodal porosity also validate previous results that demonstrated porosity saturation can occur in electrode materials with low overall total porosities relative to traditional porous carbons. We envisage that our study will guide the design of improved supercapacitors in the future.

Author Contributions

J.W.G., K.G., P.-L.T., P.S., and A.C.F. designed the research. J.W.G performed the materials synthesis and characterisation. J.W.G performed and analysed the three-electrode and two-electrode experiments. K.G. and P.-L.T. performed and analysed the EQCM experiments. All authors interpreted the results and contributed to the writing of the manuscript.

Conflicts of Interest

There are no conflicts to declare.

Data Availability

All raw experimental data files are available in the Cambridge Research Repository, Apollo, with the identifier DOI: 10.17863/CAM.105384

Acknowledgements

J.W.G. acknowledges the School of the Physical Sciences (Cambridge) for the award of an Oppenheimer Studentship. K.G. thanks a grant from the China Scholarship Council. C.J.B. acknowledges a Walters-Kundert Studentship (Selwyn College, Cambridge). A.C.F. thanks the Isaac Newton Trust of Trinity College (Cambridge) for a Research Grant (G101121), and the Yusuf Hamied Department of Chemistry (Cambridge) for the award of a BP Next Generation Fellowship. We also acknowledge an ERC Starting Grant to A.C.F., funded through the UKRI guarantee scheme (EP/X042693/1). This work was also supported by a UKRI Future Leaders Fellowship (MR/T043024/1), and a Royal Society Research Grant to A.C.F. (RGS\R2\202125). P.S. and P.-L.T. acknowledge support from the Agence Nationale de la Recherche (LabEX STORE-EX), and an ERC Synergy Grant (MoMa-STOR; ID: 951513). We thank Dr. Chris Truscott and Dr Nigel Howard for collaboration and technical expertise.

For the purpose of open access, the author has applied a Creative Commons Attribution (CC BY) licence to any Author Accepted Manuscript version arising.

References

- (1) Hmadeh, M.; Lu, Z.; Liu, Z.; Gándara, F.; Furukawa, H.; Wan, S.; Augustyn, V.; Chang, R.; Liao, L.; Zhou, F.; Perre, E.; Ozolins, V.; Suenaga, K.; Duan, X.; Dunn, B.; Yamamoto, Y.; Terasaki, O.; Yaghi, O. M. New Porous Crystals of Extended Metal-Catecholates. *Chemistry of Materials* **2012**, *24* (18), 3511–3513. <https://doi.org/10.1021/cm301194a>.
- (2) Sheberla, D.; Sun, L.; Blood-Forsythe, M. A.; Er, S.; Wade, C. R.; Brozek, C. K.; Aspuru-Guzik, A.; Dincă, M. High Electrical Conductivity in Ni₃(2,3,6,7,10,11-Hexaiminotriphenylene)₂, a Semiconducting Metal-Organic Graphene Analogue. *J Am Chem Soc* **2014**, *136* (25), 8859–8862. <https://doi.org/10.1021/ja502765n>.
- (3) Nazir, A.; Le, H. T. T.; Min, C. W.; Kasbe, A.; Kim, J.; Jin, C. S.; Park, C. J. Coupling of a Conductive Ni₃(2,3,6,7,10,11-Hexaiminotriphenylene)₂ Metal-Organic Framework with Silicon Nanoparticles for Use in High-Capacity Lithium-Ion Batteries. *Nanoscale* **2020**, *12* (3), 1629–1642. <https://doi.org/10.1039/c9nr08038d>.
- (4) Cai, D.; Lu, M.; Li, L.; Cao, J.; Chen, D.; Tu, H.; Li, J.; Han, W. A Highly Conductive MOF of Graphene Analogue Ni₃(HITP)₂ as a Sulfur Host for High-Performance Lithium–Sulfur Batteries. *Small* **2019**, *15* (44). <https://doi.org/10.1002/sml.201902605>.
- (5) Zahir Iqbal, M.; Shaheen, M.; Siddique, S.; Aftab, S.; Wabaidur, S. M. Elucidating D- π Conjugated Isoreticular 2,3,6,7,10,11-Hexahydroxytriphenylene and Hexahydroxybenzene Based Metal Organic Frameworks for Battery-Supercapacitor Hybrids. *Materials Today Sustainability* **2023**, 100415. <https://doi.org/10.1016/J.MTSUST.2023.100415>.
- (6) Gu, S.; Bai, Z.; Majumder, S.; Huang, B.; Chen, G. Conductive Metal–Organic Framework with Redox Metal Center as Cathode for High Rate Performance Lithium Ion Battery. *J Power Sources* **2019**, *429*, 22–29. <https://doi.org/10.1016/J.JPOWSOUR.2019.04.087>.
- (7) Nam, K. W.; Park, S. S.; dos Reis, R.; Dravid, V. P.; Kim, H.; Mirkin, C. A.; Stoddart, J. F. Conductive 2D Metal-Organic Framework for High-Performance Cathodes in Aqueous Rechargeable Zinc Batteries. *Nat Commun* **2019**, *10* (1). <https://doi.org/10.1038/s41467-019-12857-4>.
- (8) Dong, S.; Wu, L.; Xue, M.; Li, Z.; Xiao, D.; Xu, C.; Shen, L.; Zhang, X. Conductive Metal-Organic Framework for High Energy Sodium-Ion Hybrid Capacitors. *ACS Appl Energy Mater* **2021**, *4* (2), 1568–1574. https://doi.org/10.1021/ACSAEM.0C02758/ASSET/IMAGES/LARGE/AE0C02758_0006.JPG.
- (9) Sheberla, D.; Bachman, J. C.; Elias, J. S.; Sun, C. J.; Shao-Horn, Y.; Dincă, M. Conductive MOF Electrodes for Stable Supercapacitors with High Areal Capacitance. *Nat Mater* **2017**, *16* (2), 220–224. <https://doi.org/10.1038/nmat4766>.
- (10) Iqbal, R.; Sultan, M. Q.; Hussain, S.; Hamza, M.; Tariq, A.; Akbar, M. B.; Ma, Y.; Zhi, L. The Different Roles of Cobalt and Manganese in Metal-Organic Frameworks for Supercapacitors. *Adv Mater Technol* **2021**, 2000941. <https://doi.org/10.1002/admt.202000941>.
- (11) Feng, D.; Lei, T.; Lukatskaya, M. R.; Park, J.; Huang, Z.; Lee, M.; Shaw, L.; Chen, S.; Yakovenko, A. A.; Kulkarni, A.; Xiao, J.; Fredrickson, K.; Tok, J. B.; Zou, X.; Cui, Y.; Bao,

- Z. Robust and Conductive Two-Dimensional Metal–Organic Frameworks with Exceptionally High Volumetric and Areal Capacitance. *Nat Energy* **2018**, *3*, 30–36.
<https://doi.org/10.1038/s41560-017-0044-5>.
- (12) Banda, H.; Dou, J. H.; Chen, T.; Libretto, N. J.; Chaudhary, M.; Bernard, G. M.; Miller, J. T.; Michaelis, V. K.; Dincă, M. High-Capacitance Pseudocapacitors from Li⁺-Ion Intercalation in Nonporous, Electrically Conductive 2D Coordination Polymers. *J Am Chem Soc* **2021**, *143* (5), 2285–2292.
https://doi.org/10.1021/JACS.0C10849/SUPPL_FILE/JA0C10849_SI_001.PDF.
- (13) Li, W. H.; Ding, K.; Tian, H. R.; Yao, M. S.; Nath, B.; Deng, W. H.; Wang, Y.; Xu, G. Conductive Metal–Organic Framework Nanowire Array Electrodes for High-Performance Solid-State Supercapacitors. *Adv Funct Mater* **2017**, *27* (27).
<https://doi.org/10.1002/adfm.201702067>.
- (14) Gittins, J. W.; Balhatchet, C. J.; Chen, Y.; Liu, C.; Madden, D. G.; Britto, S.; Golomb, M. J.; Walsh, A.; Fairen-Jimenez, D.; Dutton, S. E.; Forse, A. C. Insights into the Electric Double-Layer Capacitance of Two-Dimensional Electrically Conductive Metal–Organic Frameworks. *J Mater Chem A Mater* **2021**, *9* (29), 16006–16015. <https://doi.org/10.1039/D1TA04026J>.
- (15) Gittins, J. W.; Balhatchet, C. J.; Fairclough, S. M.; Forse, A. C. Enhancing the Energy Storage Performances of Metal–Organic Frameworks by Controlling Microstructure. *Chem Sci* **2022**, *13* (32), 9210–9219. <https://doi.org/10.1039/D2SC03389E>.
- (16) Wrogemann, J. M.; Lüther, M. J.; Bärman, P.; Lounasvuori, M.; Javed, A.; Tiemann, M.; Golnak, R.; Xiao, J.; Petit, T.; Placke, T.; Winter, M. Overcoming Diffusion Limitation of Faradaic Processes: Property-Performance Relationships of 2D Conductive Metal-Organic Framework Cu₃(HHTP)₂ for Reversible Lithium-Ion Storage. *Angewandte Chemie International Edition* **2023**, e202303111. <https://doi.org/10.1002/ANIE.202303111>.
- (17) Borysiewicz, M. A.; Dou, J. H.; Stassen, I.; Dincă, M. Why Conductivity Is Not Always King – Physical Properties Governing the Capacitance of 2D Metal–Organic Framework-Based EDLC Supercapacitor Electrodes: A Ni₃(HITP)₂ Case Study. *Faraday Discuss* **2021**, *231* (0), 298–304. <https://doi.org/10.1039/D1FD00028D>.
- (18) Shin, S.-J.; Gittins, J. W.; Balhatchet, C. J.; Walsh, A.; Forse, A. C.; Shin, S.-J.; Gittins, J. W.; Balhatchet, C. J.; Forse, A. C.; Walsh, A. Metal–Organic Framework Supercapacitors: Challenges and Opportunities. *Adv Funct Mater* **2023**, 2308497.
<https://doi.org/10.1002/ADFM.202308497>.
- (19) Chmiola, J.; Largeot, C.; Taberna, P. L.; Simon, P.; Gogotsi, Y. Desolvation of Ions in Subnanometer Pores and Its Effect on Capacitance and Double-Layer Theory. *Angewandte Chemie - International Edition* **2008**, *47* (18), 3392–3395.
<https://doi.org/10.1002/anie.200704894>.
- (20) Chmiola, J.; Yushin, G.; Gogotsi, Y.; Portet, C.; Simon, P.; Taberna, P. L. Anomalous Increase in Carbon at Pore Sizes Less than 1 Nanometer. *Science (1979)* **2006**, *313* (5794), 1760–1763. <https://doi.org/10.1126/science.1132195>.
- (21) Largeot, C.; Portet, C.; Chmiola, J.; Taberna, P. L.; Gogotsi, Y.; Simon, P. Relation between the Ion Size and Pore Size for an Electric Double-Layer Capacitor. *J Am Chem Soc* **2008**, *130* (9), 2730–2731. <https://doi.org/10.1021/ja7106178>.

- (22) Jäckel, N.; Simon, P.; Gogotsi, Y.; Presser, V. Increase in Capacitance by Subnanometer Pores in Carbon. *ACS Energy Lett* **2016**, *1* (6), 1262–1265. https://doi.org/10.1021/ACSENERGYLETT.6B00516/ASSET/IMAGES/LARGE/NZ-2016-005167_0003.JPEG.
- (23) Centeno, T. A.; Sereda, O.; Stoeckli, F. Capacitance in Carbon Pores of 0.7 to 15 Nm: A Regular Pattern. *Physical Chemistry Chemical Physics* **2011**, *13* (27), 12403–12406. <https://doi.org/10.1039/c1cp20748b>.
- (24) Stoeckli, F.; Centeno, T. A. Optimization of the Characterization of Porous Carbons for Supercapacitors. *J Mater Chem A Mater* **2013**, *1*, 6865–6873. <https://doi.org/10.1039/c3ta10906b>.
- (25) García-Gómez, A.; Moreno-Fernández, G.; Lobato, B.; Centeno, T. A. Constant Capacitance in Nanopores of Carbon Monoliths. *Physical Chemistry Chemical Physics* **2015**, *17* (24), 15687–15690. <https://doi.org/10.1039/C5CP01904D>.
- (26) Jäckel, N.; Rodner, M.; Schreiber, A.; Jeongwook, J.; Zeiger, M.; Aslan, M.; Weingarh, D.; Presser, V. Anomalous or Regular Capacitance? The Influence of Pore Size Dispersity on Double-Layer Formation. *J Power Sources* **2016**, *326*, 660–671. <https://doi.org/10.1016/J.JPOWSOUR.2016.03.015>.
- (27) Mysyk, R.; Raymundo-Piñero, E.; Pernak, J.; Béguin, F. Confinement of Symmetric Tetraalkylammonium Ions in Nanoporous Carbon Electrodes of Electric Double-Layer Capacitors. *Journal of Physical Chemistry C* **2009**, *113* (30), 13443–13449. https://doi.org/10.1021/JP901539H/ASSET/IMAGES/JP-2009-01539H_M007.GIF.
- (28) Lukatskaya, M. R.; Feng, D.; Bak, S.-M.; To, J. W. F.; Yang, X.-Q.; Cui, Y.; Feldblyum, J. I.; Bao, Z. Understanding the Mechanism of High Capacitance in Nickel Hexaaminobenzene-Based Conductive Metal–Organic Frameworks in Aqueous Electrolytes. *ACS Nano* **2020**, *acs.nano.0c07292*. <https://doi.org/10.1021/acsnano.0c07292>.
- (29) Bi, S.; Banda, H.; Chen, M.; Niu, L.; Chen, M.; Wu, T.; Wang, J.; Wang, R.; Feng, J.; Chen, T.; Dincă, M.; Kornyshev, A. A.; Feng, G. Molecular Understanding of Charge Storage and Charging Dynamics in Supercapacitors with MOF Electrodes and Ionic Liquid Electrolytes. *Nat Mater* **2020**, *19* (5), 552–558. <https://doi.org/10.1038/s41563-019-0598-7>.
- (30) Shin, S.-J.; Gittins, J. W.; Golomb, M. J.; Forse, A. C.; Walsh, A. Microscopic Origin of Electrochemical Capacitance in Metal–Organic Frameworks. *J Am Chem Soc* **2023**, *145*, 57. https://doi.org/10.1021/JACS.3C04625/ASSET/IMAGES/LARGE/JA3C04625_0007.JPEG.
- (31) He, L.; Yang, L.; Dincă, M.; Zhang, R.; Li, J. Observation of Ion Electrosorption in Metal–Organic Framework Micropores with In Operando Small-Angle Neutron Scattering. *Angewandte Chemie - International Edition* **2020**, *59* (24), 9773–9779. <https://doi.org/10.1002/anie.201916201>.
- (32) Levi, M. D.; Levy, N.; Sigalov, S.; Salitra, G.; Aurbach, D.; Maier, J. Electrochemical Quartz Crystal Microbalance (EQCM) Studies of Ions and Solvents Insertion into Highly Porous Activated Carbons. *J Am Chem Soc* **2010**, *132* (38), 13220–13222. https://doi.org/10.1021/JA104391G/SUPPL_FILE/JA104391G_SI_001.PDF.
- (33) Levi, M. D.; Sigalov, S.; Salitra, G.; Aurbach, D.; Maier, J. The Effect of Specific Adsorption of Cations and Their Size on the Charge-Compensation Mechanism in Carbon Micropores:

- The Role of Anion Desorption. *ChemPhysChem* **2011**, *12* (4), 854–862.
<https://doi.org/10.1002/CPHC.201000653>.
- (34) Tsai, W. Y.; Taberna, P. L.; Simon, P. Electrochemical Quartz Crystal Microbalance (EQCM) Study of Ion Dynamics in Nanoporous Carbons. *J Am Chem Soc* **2014**, *136* (24), 8722–8728.
https://doi.org/10.1021/JA503449W/SUPPL_FILE/JA503449W_SI_001.PDF.
- (35) Zhang, E.; Wu, Y. C.; Shao, H.; Klimavicius, V.; Zhang, H.; Taberna, P. L.; Grothe, J.; Buntkowsky, G.; Xu, F.; Simon, P.; Kaskel, S. Unraveling the Capacitive Charge Storage Mechanism of Nitrogen-Doped Porous Carbons by EQCM and SsNMR. *J Am Chem Soc* **2022**, *144* (31), 14217–14225.
https://doi.org/10.1021/JACS.2C04841/ASSET/IMAGES/LARGE/JA2C04841_0004.JPEG.
- (36) Levi, M. D.; Lukatskaya, M. R.; Sigalov, S.; Beidaghi, M.; Shpigel, N.; Daikhin, L.; Aurbach, D.; Barsoum, M. W.; Gogotsi, Y. Solving the Capacitive Paradox of 2D MXene Using Electrochemical Quartz-Crystal Admittance and In Situ Electronic Conductance Measurements. *Adv Energy Mater* **2015**, *5* (1), 1400815.
<https://doi.org/10.1002/AENM.201400815>.
- (37) Cheng, S.; Gao, W.; Cao, Z.; Yang, Y.; Xie, E.; Fu, J. Selective Center Charge Density Enables Conductive 2D Metal–Organic Frameworks with Exceptionally High Pseudocapacitance and Energy Density for Energy Storage Devices. *Advanced Materials* **2022**, *34* (14), 2109870. <https://doi.org/10.1002/ADMA.202109870>.
- (38) Hoppe, B.; Hindricks, K. D. J.; Warwas, D. P.; Schulze, H. A.; Mohmeyer, A.; Pinkvos, T. J.; Zailskas, S.; Krey, M. R.; Belke, C.; König, S.; Fröba, M.; Haug, R. J.; Behrens, P. Graphene-like Metal-Organic Frameworks: Morphology Control, Optimization of Thin Film Electrical Conductivity and Fast Sensing Applications. *CrystEngComm* **2018**, *20* (41), 6458–6471.
<https://doi.org/10.1039/c8ce01264d>.
- (39) Thommes, M.; Kaneko, K.; Neimark, A. V.; Olivier, J. P.; Rodriguez-Reinoso, F.; Rouquerol, J.; Sing, K. S. W. Physisorption of Gases, with Special Reference to the Evaluation of Surface Area and Pore Size Distribution (IUPAC Technical Report). *Pure and Applied Chemistry* **2015**, *87* (9–10), 1051–1069. <https://doi.org/10.1515/PAC-2014-1117/PDF>.
- (40) Duan, P.; Moreton, J. C.; Tavares, S. R.; Semino, R.; Maurin, G.; Cohen, S. M.; Schmidt-Rohr, K. Polymer Infiltration into Metal-Organic Frameworks in Mixed-Matrix Membranes Detected in Situ by NMR. *J Am Chem Soc* **2019**, *141* (18), 7589–7595.
https://doi.org/10.1021/JACS.9B02789/ASSET/IMAGES/LARGE/JA-2019-02789G_0005.JPEG.
- (41) Abbas, Q.; Pajak, D.; Frąckowiak, E.; Béguin, F. Effect of Binder on the Performance of Carbon/Carbon Symmetric Capacitors in Salt Aqueous Electrolyte. *Electrochim Acta* **2014**, *140*, 132–138. <https://doi.org/10.1016/J.ELECTACTA.2014.04.096>.
- (42) Maarof, H. I.; Daud, W. M. A. W.; Aroua, M. K. Effect of Varying the Amount of Binder on the Electrochemical Characteristics of Palm Shell Activated Carbon. *IOP Conf. Ser.: Mater. Sci. Eng.* **2017**, *210* (012011). <https://doi.org/10.1088/1757-899X/210/1/012011>.
- (43) Ue, M. Mobility and Ionic Association of Lithium and Quaternary Ammonium Salts in Propylene Carbonate and γ -Butyrolactone. *J Electrochem Soc* **1994**, *141* (12), 3336–3342.
<https://doi.org/10.1149/1.2059336/XML>.

- (44) Kubota, S.; Ozaki, S.; Onishi, J.; Kano, K.; Shirai, O. Selectivity on Ion Transport across Bilayer Lipid Membranes in the Presence of Gramicidin A. *Analytical Sciences* **2009**, *25* (2), 189–194. <https://doi.org/10.2116/ANALSCI.25.189/METRICS>.
- (45) Gittins, J. W.; Chen, Y.; Arnold, S.; Augustyn, V.; Balducci, A.; Brousse, T.; Frackowiak, E.; Gómez-Romero, P.; Kanwade, A.; Köps, L.; Jha, P. K.; Lyu, D.; Meo, M.; Pandey, D.; Pang, L.; Presser, V.; Rapisarda, M.; Rueda-García, D.; Saeed, S.; Shirage, P. M.; Ślesiński, A.; Soavi, F.; Thomas, J.; Titirici, M.-M.; Wang, H.; Xu, Z.; Yu, A.; Zhang, M.; Forse, A. C. Interlaboratory Study Assessing the Analysis of Supercapacitor Electrochemistry Data. *J Power Sources* **2023**, *585*, 233637. <https://doi.org/10.1016/J.JPOWSOUR.2023.233637>.
- (46) Banda, H.; Périé, S.; Daffos, B.; Dubois, L.; Crosnier, O.; Simon, P.; Taberna, P. L.; Duclairoir, F. Investigation of Ion Transport in Chemically Tuned Pillared Graphene Materials through Electrochemical Impedance Analysis. *Electrochim Acta* **2019**, *296*, 882–890. <https://doi.org/10.1016/J.ELECTACTA.2018.11.122>.
- (47) Banda, H.; Daffos, B.; Périé, S.; Chenavier, Y.; Dubois, L.; Aradilla, D.; Pouget, S.; Simon, P.; Crosnier, O.; Taberna, P. L.; Duclairoir, F. Ion Sieving Effects in Chemically Tuned Pillared Graphene Materials for Electrochemical Capacitors. *Chemistry of Materials* **2018**, *30* (9), 3040–3047. https://doi.org/10.1021/ACS.CHEMMATER.8B00759/ASSET/IMAGES/LARGE/CM-2018-00759Q_0004.JPEG.
- (48) Ren, C. E.; Hatzell, K. B.; Alhabeb, M.; Ling, Z.; Mahmoud, K. A.; Gogotsi, Y. Charge- and Size-Selective Ion Sieving Through Ti₃C₂T_x MXene Membranes. *Journal of Physical Chemistry Letters* **2015**, *6* (20), 4026–4031. https://doi.org/10.1021/ACS.JPCLETT.5B01895/ASSET/IMAGES/LARGE/JZ-2015-018957_0004.JPEG.
- (49) Sauerbrey, G. Verwendung von Schwingquarzen Zur Wägung Dünner Schichten Und Zur Mikrowägung. *Zeitschrift für Physik* **1959**, *155* (2), 206–222. <https://doi.org/10.1007/BF01337937/METRICS>.
- (50) Levi, M. D.; Salitra, G.; Levy, N.; Aurbach, D.; Maier, J. Application of a Quartz-Crystal Microbalance to Measure Ionic Fluxes in Microporous Carbons for Energy Storage. *Nature Materials* **2009**, *8* (11), 872–875. <https://doi.org/10.1038/nmat2559>.
- (51) Deschamps, M.; Gilbert, E.; Azais, P.; Raymundo-Piñero, E.; Ammar, M. R.; Simon, P.; Massiot, D.; Béguin, F. Exploring Electrolyte Organization in Supercapacitor Electrodes with Solid-State NMR. *Nat Mater* **2013**, *12* (4), 351–358. <https://doi.org/10.1038/NMAT3567>.
- (52) Borchardt, L.; Oschatz, M.; Paasch, S.; Kaskel, S.; Brunner, E. Interaction of Electrolyte Molecules with Carbon Materials of Well-Defined Porosity: Characterization by Solid-State NMR Spectroscopy. *Physical Chemistry Chemical Physics* **2013**, *15* (36), 15177–15184. <https://doi.org/10.1039/C3CP52283K>.
- (53) Levi, M. D.; Sigalov, S.; Salitra, G.; Aurbach, D.; Maier, J. The Effect of Specific Adsorption of Cations and Their Size on the Charge-Compensation Mechanism in Carbon Micropores: The Role of Anion Desorption. *ChemPhysChem* **2011**, *12* (4), 854–862. <https://doi.org/10.1002/CPHC.201000653>.

- (54) Zhang, K.; Zhou, G.; Fang, T.; Jiang, K.; Liu, X. Structural Reorganization of Ionic Liquid Electrolyte by a Rapid Charge/Discharge Circle. *Journal of Physical Chemistry Letters* **2021**, *12* (9), 2273–2278.
https://doi.org/10.1021/ACS.JPCLETT.1C00156/SUPPL_FILE/JZ1C00156_SI_001.PDF.
- (55) Wen, R.; Rahn, B.; Magnussen, O. M. Potential-Dependent Adlayer Structure and Dynamics at the Ionic Liquid/Au(111) Interface: A Molecular-Scale In Situ Video-STM Study. *Angewandte Chemie International Edition* **2015**, *54* (20), 6062–6066.
<https://doi.org/10.1002/ANIE.201501715>.
- (56) Mao, X.; Brown, P.; Červinka, C.; Hazell, G.; Li, H.; Ren, Y.; Chen, D.; Atkin, R.; Eastoe, J.; Grillo, I.; Padua, A. A. H.; Costa Gomes, M. F.; Hatton, T. A. Self-Assembled Nanostructures in Ionic Liquids Facilitate Charge Storage at Electrified Interfaces. *Nature Materials* **2019**, *18*:12 **2019**, *18* (12), 1350–1357. <https://doi.org/10.1038/s41563-019-0449-6>.
- (57) Feng, G.; Huang, J.; Sumpter, B. G.; Meunier, V.; Qiao, R. Structure and Dynamics of Electrical Double Layers in Organic Electrolytes. *Physical Chemistry Chemical Physics* **2010**, *12* (20), 5468–5479. <https://doi.org/10.1039/C000451K>.
- (58) Yang, P. Y.; Ju, S. P.; Hsieh, H. S.; Lin, J. Sen. The Diffusion Behavior and Capacitance of Tetraethylammonium/Tetrafluoroborate Ions in Acetonitrile with Different Molar Concentrations: A Molecular Dynamics Study. *RSC Adv* **2017**, *7* (87), 55044–55050.
<https://doi.org/10.1039/C7RA09465E>.
- (59) Chmiola, J.; Largeot, C.; Taberna, P. L.; Simon, P.; Gogotsi, Y. Desolvation of Ions in Subnanometer Pores and Its Effect on Capacitance and Double-Layer Theory. *Angewandte Chemie International Edition* **2008**, *47* (18), 3392–3395.
<https://doi.org/10.1002/ANIE.200704894>.